frontiers in Earth Science

ORIGINAL RESEARCH
published: 02 March 2022
doi: 10.3389/feart.2022.843521

Numerical Simulations of Combined Brine Flooding With Electrical Heating–Assisted Depressurization for Exploitation of Natural Gas Hydrate in the Shenhu Area of the South China Sea

Qi Zhang[1,2,3] *and Yanfei Wang*[1,2,3]*

[1]Key Laboratory of Petroleum Resources Research, Institute of Geology and Geophysics, Chinese Academy of Sciences, Beijing, China, [2]College of Earth and Planetary Sciences, University of Chinese Academy of Sciences, Beijing, China, [3]Innovation Academy for Earth Science, Chinese Academy of Sciences, Beijing, China

OPEN ACCESS

Edited by:
Pibo Su,
Guangzhou Marine Geological Survey, China

Reviewed by:
Bo Li,
Chongqing University, China
Xianying Wang,
Guangzhou Marine Geological Survey, China
Cheng Lu,
China Geological Survey, China

***Correspondence:**
Yanfei Wang
yfwang@mail.iggcas.ac.cn

Specialty section:
This article was submitted to Economic Geology, a section of the journal Frontiers in Earth Science

Received: *04 January 2022*
Accepted: *07 February 2022*
Published: *02 March 2022*

Citation:
Zhang Q and Wang Y (2022) Numerical Simulations of Combined Brine Flooding With Electrical Heating–Assisted Depressurization for Exploitation of Natural Gas Hydrate in the Shenhu Area of the South China Sea. Front. Earth Sci. 10:843521. doi: 10.3389/feart.2022.843521

The Shenhu area of the South China Sea (SCS) is one of the most promising fields for natural gas hydrate (NGH) exploitation. However, previous studies conclude that using only depressurization is inefficient for this challenging hydrate deposits surrounded by permeable water zones, which requires assistance by thermal stimulation to promote hydrate decomposition and methane recovery. However, traditional thermal stimulation methods with hot water or steam injection induce massive heat loss along the wellbore. In addition, *in situ* electrical heating only results in a limited high temperature region due to low thermal conductivity of hydrate deposits. Therefore, we numerically investigate the performance of combined brine flooding with electrical heating–assisted depressurization in horizontal wells for exploitation of natural gas hydrate in the SCS, which simultaneously possesses the merits of low heat loss and enhanced heat transfer by convection. Our simulation results show that thermal stimulation by combined brine flooding with electrical heating can significantly enhance hydrate dissociation and methane recovery. After 20 years of production, the cumulative methane production of combined brine flooding with electrical heating–assisted depressurization is 1.41 times of that conducted by the only depressurization method. Moreover, the energy efficiency can be improved by reducing electrical heating time, and terminating electrical heating with 70% hydrate dissociation achieves the highest net energy gain. In addition, methane recovery and net energy gain increases with electrical heating power and brine injection pressure but with a decreasing rate. Therefore, the selection of electrical heating power and brine injection pressure should be performed carefully and comprehensively considering both the efficiency of gas production and risks of geological hazard. It is hoped that our research results will provide reference and guidance for the development of a similar NGH reservoir in order to promote the industrial development process of NGH.

Keywords: natural gas hydrate, numerical simulations, brine injection, electrical heating, depressurization, Shenhu area

INTRODUCTION

Natural gas hydrates are crystalline substances comprising water molecules and gas molecules, in which a solid water lattice accommodates gas molecules in a cage-like structure (Sloan, 2003; Wang et al., 2017; Wu et al., 2020). The most typical hydrate-forming gas is methane, and NGH mainly occurs in terrestrial permafrost and offshore sediments where low temperature and high-pressure conditions needed by hydrate stabilization are met (Collett, 2002; Koh, 2002; Chong et al., 2016). As a potential new unconventional energy, NGHs are currently attracting significant attention owing to their extensive distribution, great resource potential, high energy density, and low environmental pollution (Koh et al., 2012; Yang et al., 2018). Current estimations of the hydrate-containing hydrocarbon gas available at standard conditions ranges from 10^{15} to 10^{18} m^3, which is twice as much as the conventional fossil energy (Moridis et al., 2009a). If NGH can be exploited in a safe and efficient way to produce natural gas and replace traditional fossil fuels, the problem of global energy shortage and environmental pollution can be greatly alleviated (Liang et al., 2020; Yin et al., 2020).

The Shenhu area on the northern continental slope of the South China Sea (SCS) is one of the most promising fields for gas hydrate exploitation. In 2007, 2015, and 2016, three gas hydrate drilling expeditions (GMGS1, 3, and 4) were conducted in this area by the Guangzhou Marine Geological Survey (Wu and Wang, 2018). During the GMGS1, five sites were selected for deep drilling and sampling in the Shenhu area (**Figure 1**), among which three sites (SH2, SH3, and SH7) were verified with the existence of methane gas hydrates by depressurization experiments (Wu et al., 2011). Since then, many numerical simulations were carried out on hydrate production in the Shenhu area, including the SH2 site (Su et al., 2011; Su et al., 2012b; Su et al., 2013; Jin et al., 2016), SH3 site (Su et al., 2012a), and SH7 site (Li et al., 2010; Li et al., 2011; Li et al., 2013; Sun et al., 2015). These simulations include different production methods, such as depressurization and thermal stimulation, the use of vertical and horizontal wells, the effects of the underlying and overburden layer permeability, and other aspects related to hydrate production (Sun et al., 2019). Based on aforementioned numerical studies and many other laboratory experiments on the NGH in the SCS, the China Geological Survey successfully conducted the first and second production tests in the Shenhu area of the SCS in 2017 and 2020, respectively, using a vertical well and a horizontal well. The first production test lasted for 60 days with a cumulative gas production of 3.09×10^5 m^3 (Li et al., 2018b), and the second production test achieved 30 days of continuous gas production, with a cumulative gas production of 8.614×10^5 m^3, whose average daily gas production is 5.57 times as much as that obtained in the first production test (Ye et al., 2020). The two successful production tests proved the technical feasibility of gas production from the clayey silt NGH reservoir, which accounts for 90% of the total hydrate reservoirs but tend to be the most difficult to exploit owing to low permeability and high content of clay (Boswell and Collett, 2011).

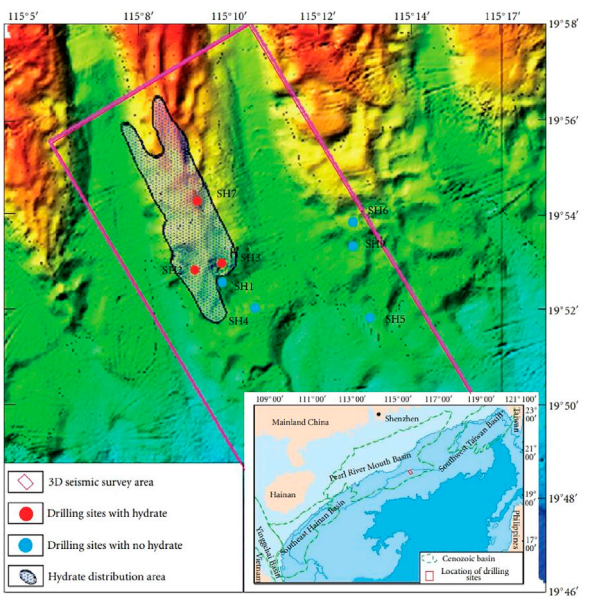

FIGURE 1 | Location of study area, drilling sites, and the confirmed gas hydrate distribution in the Shenhu area. Insert: General location of study area in the northern slope of the South China Sea (Wu et al., 2011).

To exploit the NGH, the equilibrium state of the reservoirs should be broken by certain mechanisms, leading to *in situ* dissociation of the NGH into gas and water; then the gas–water mixture can be extracted and gas–liquid separation can be conducted successively (Konno et al., 2016). According to the phase equilibrium curve of the NGH, those certain mechanisms include the following: depressurization (Moridis et al., 2007; Moridis et al., 2009b; Sun et al., 2015; Yang et al., 2019); thermal stimulation (Moridis et al., 2004; Wang et al., 2018; Liu et al., 2020); use of inhibitors (Sung et al., 2002); and gas molecule exchange (White et al., 2011; Koh et al., 2016; Zhang et al., 2017). Currently, depressurization is considered to be the most economical and efficient method for NGH exploitation (Oyama et al., 2012; Chong et al., 2017), which was used in the first and second production tests in the Shenhu area of the SCS. However, there are also problems attached to this method, such as small influence range and rapid drop of the gas production rate. Hydrate decomposition is an endothermic reaction, but the only heat sources of NGH exploitation by depressurization are the sensible heat of the hydrate deposit, the heat transferred from the surroundings, and the latent heat released by the phase transition from water to ice (Zhao et al., 2014). Due to insufficient heat supply, the reservoir temperature will significantly reduce which may lead to the formation of ice and secondary hydrate, hindering the recovery of methane (Wang et al., 2020). Therefore, thermal stimulation methods are usually used in company with depressurization to provide additional heat for the hydrate deposit and accelerate NGH dissociation (Wan et al., 2018).

Traditional thermal stimulation methods utilize hot water and steam injection, which can be implemented in the form of the huff and puff method, hot water/steam flooding, and hot water/steam-assisted gravity drainage (SAGD). Actually, these methods have

widely been used in the field of thermal enhanced oil recovery and provide a significant amount of oil in the overall global oil outlook (Mokheimer et al., 2019). Many authors also evaluated the potential of these methods in promoting methane production from the NGH by laboratory experiments and numerical simulations. Li et al. (2011) and Su et al. (2012b) numerically investigated the gas production performance by the huff and puff method in the Shenhu area, and the results showed that the gas production rate was very low and the secondary hydrate formation occurs during the injection stage. In addition, Feng et al. (2013) and Feng et al. (2014) compared the gas production potential of depressurization combined with warm brine injection by different dual horizontal well configurations, respectively, corresponding to the flooding method (dual horizontal wells in the same horizontal plane) and the SAGD method (dual horizontal wells in the same vertical plane). They concluded that the average gas production rate of the flooding method exceeds the commercially viable production rate in the Gulf of Mexico, which is more favorable than the SAGD method. In addition, Jin et al. (2016) also proved that gas recovery can be improved significantly by hot water flooding for the hydrate deposits in the Shenhu area, and the well spacing affects the methane production significantly when thermal stimulation starts. However, when hot water or steam is injected, the heat loss along the wellbore is considerable even with insulated tubing, after hundreds or even thousands of meter transportation from the surface or ocean to the hydrate-bearing layers (hereafter, referred to as HBL) (Li et al., 2018a).

To overcome the shortcoming of traditional hot water/steam flooding method, novel thermal stimulation methods of electrical or electromagnetic heating and methane *in situ* combustion have been proposed, which generate heat directly in the formation to avoid wellbore heat loss. In this study, we focus on electrical heating, and many laboratory experiments have been conducted to clarify the effects of electrical heating–assisted depressurization on hydrate dissociation and methane recovery (Falser et al., 2012; Li et al., 2018a; Liang et al., 2018; Minagawa et al., 2018; Wan et al., 2020a; Wan et al., 2020b; He et al., 2021). For example, Li et al. (2018b) found that the production efficiency of depressurization can be greatly enhanced by using the electrical heating simultaneously for the methane hydrate in a cuboid pressure vessel. In their experiment, a resistance heating wire is distributed uniformly in the inner surface of the well, and the whole well can be heated evenly when direct current is supplied to the wire. On the other hand, electrical heating was performed through the application of alternating current using two end caps as a pair of electrodes in the experiments by Minagawa et al. (2018), which suppressed the decrease in the temperature of NGH sediment core and enabled higher gas production when combined with depressurization. In addition, Wan et al. (2020b) proposed a novel tripartite strategy of electrical resistance heating, room temperature water flooding, and depressurization which combines the advantages of simultaneously reducing heat loss and enhanced heat transfer by convection and results in the best energy recovery efficiency among different thermal stimulation modes in a high-pressure reactor using two vertical wells. In addition to laboratory experiments, several numerical simulations were also conducted on the gas production of hydrate dissociation by electrical heating combined with depressurization (Wan et al., 2020a; Li et al., 2020; Zhao et al., 2021; Liu et al., 2022), but mainly performed in the laboratory scale. Wan et al. (2020a) conducted simulations of wellbore heating with depressurization for gas production from hydrate sediments in a rectangular cylinder model. Their results showed that a combination of depressurization and wellbore heating is more favorable for the enhancement of heat transfer and faster energy recovery. Similarly, in a laboratory-scale axisymmetric model, Liu et al. (2022) conducted simulations on the gas production behavior from the depressurization-induced dissociation of methane hydrate by electrical heating and on the optimization of the electrical heating scheme to achieve high-efficient utilization of electrical energy. However, the numerical simulations in the reservoir scale are rare, and recently Zhao et al. (2021) numerically evaluated the production performance of the low-frequency electrical heating–assisted depressurization (LF-EHAD) method for methane recovery from hydrate deposits in the Shenhu area of the SCS. In addition, the LF-EHAD method significantly enhances hydrate dissociation and gas production over the depressurization method and outperforms hot water flooding in higher energy utilization efficiency. Due to the large gap between laboratory and reservoir conditions, it is necessary to further numerically investigate the methane production from the NGH by electrical heating–assisted depressurization in field scale.

Therefore, the goal of this study is to numerically evaluate the performance of the combined brine flooding with electrical heating–assisted depressurization for hydrate exploitation in the Shenhu area of the SCS. The tripartite exploitation strategy with brine injection given by Wan et al. (2020b) is utilized because the simulation results of hydrate exploitation in field scale by *in situ* electrical heating show limitation of the high-temperature region and existing mainly near the heating wellbore due to the low thermal conductivity of hydrate deposits (Li et al., 2020). In consideration of the obvious advantages of horizontal wells over vertical wells, such as increasing single-well controlled reserves and gas production and reducing the risks of generating secondary hydrates and freezing (Feng et al., 2015; Ye et al., 2020), we adopt the same well configuration as done by Feng et al. (2014), that is, horizontal wells in the same horizontal plane. In addition, the pure depressurization method is also conducted as a comparison. In order to optimize the novel tripartite strategy, numerical results of methane recovery, water production and energy efficiency from different electrical heating times and power, and brine injection pressure are provided in detail and comprehensively analyzed. It is hoped that our numerical results in this study will provide reference and guidance for the development of similar low-permeability marine clayey–silt NGH with permeable surrounding water zones.

MATERIALS AND METHODS

Geological Setting of Study Area

The Shenhu area is near southeast of Shenhu Underwater Sandy Bench in the middle of the north slope of the SCS, between Xisha Trough and Dongsha Islands. Tectonically, the research area is

located in the Zhu II Depression, Pearl River Mouth Basin (**Figure 1**), which has been in the process of tectonic subsidence since the middle Miocene along with a high sedimentation rate, providing abundant organic matter (producing methane by pyrolysis or biological action) for the NGH (Wu et al., 2010). Large-scale mud diapirs, vertical fissure systems, and highly angled fractures were formed by tectonic movements, which can provide conduits for gas migration (Sun et al., 2019). The bottom temperature of the Shenhu area is 3.3–3.7°C with a geothermal gradient of 45–67°C/km, and the bottom pressure is more than 10 MPa (Yang et al., 2010; Sun et al., 2015), which meets the favorable temperature and pressure conditions for the formation of the hydrate reservoir. Therefore, this area becomes one of the most promising fields for gas hydrate exploitation.

In this study, we focused on the hydrate deposits that occur at the site SH2 drilled in GMGS1 because of high hydrate saturation and substantial amount of available data. The water depth at SH2 is 1,235 m. The HBL is 40 m thick overlain by a permeable overburden of 188 m thick and underlain by a permeable zone of mobile water. Based on the drilling and sampling data, the hydrate saturation ranges from 25 to 48%, and the porosity ranges from 0.33 to 0.48, which implies that a huge amount of natural gas is stored in the hydrate deposits. The hydrate disseminates in the sediments that mainly comprise silty clay and clay silt. In addition, it is detected that the gases contained in the hydrate in SH2 mainly consist of methane (96.10–99.91%) with minor quantities of ethane and propane (Wu et al., 2010).

Model Setup and Well Configuration

Based on the geological setting of SH2 of the Shenhu area in the SCS, the established conceptual model for numerical simulation and well configuration is shown in **Figure 2A**. The conceptual model consists of three horizontal layers including the 40-m-thick HBL and 30-m-thick permeable overburden and underburden water-bearing stratums (100 m in total), which are thought to be sufficient to accurately calculate the heat transfer to the HBL during the 20 years of production (Moridis and Reagan, 2011). The hydrate in the HBL is assumed to only comprise methane with a saturation of 0.4, and the remaining pore space is occupied by water with a saturation of 0.6. The porosity and intrinsic permeability of the HBL are, respectively, 0.38 and 10 millidarcy (mD). Due to lack of relevant information, the lithology of the surrounding water-bearing stratums is assumed to be same as the HBL but lacking hydrate. The values of simulation parameters used in our numerical model are summarized in **Table 1**.

As shown in **Figure 2A**, three horizontal wells are adopted in our study considering their obvious advantages over vertical wells, such as increasing single-well controlled reserves and gas production and reducing the risks of generating secondary hydrates and freezing (Feng et al., 2015; Ye et al., 2020). In order to avoid water and gas leakage, the vertical part of wells is sealed and the opened horizontal part with a length of 1,000 m is located at the middle of the HBL. Same as the study by Moridis et al. (2013), the interior of the wells is defined as pseudo porous media approximately, which has a high porosity of 1.0, a high permeability of 1.0×10^{-6} m^{2,} and a low capillary pressure of 0. Two side wells are conducted at a constant pressure to produce methane for the whole exploitation period (20 years). However, the middle well is first used to depressurize for 5 years in order to dissociate the hydrate and increase the permeability around the well. Then, thermal simulation starts by the flowing electric current through the resistance wire around the middle well. At the same time, a brine of 20°C (directly from sea) is also injected into hydrate formation at a constant pressure by the middle well, which can carry the electrical heat deep into the HBL.

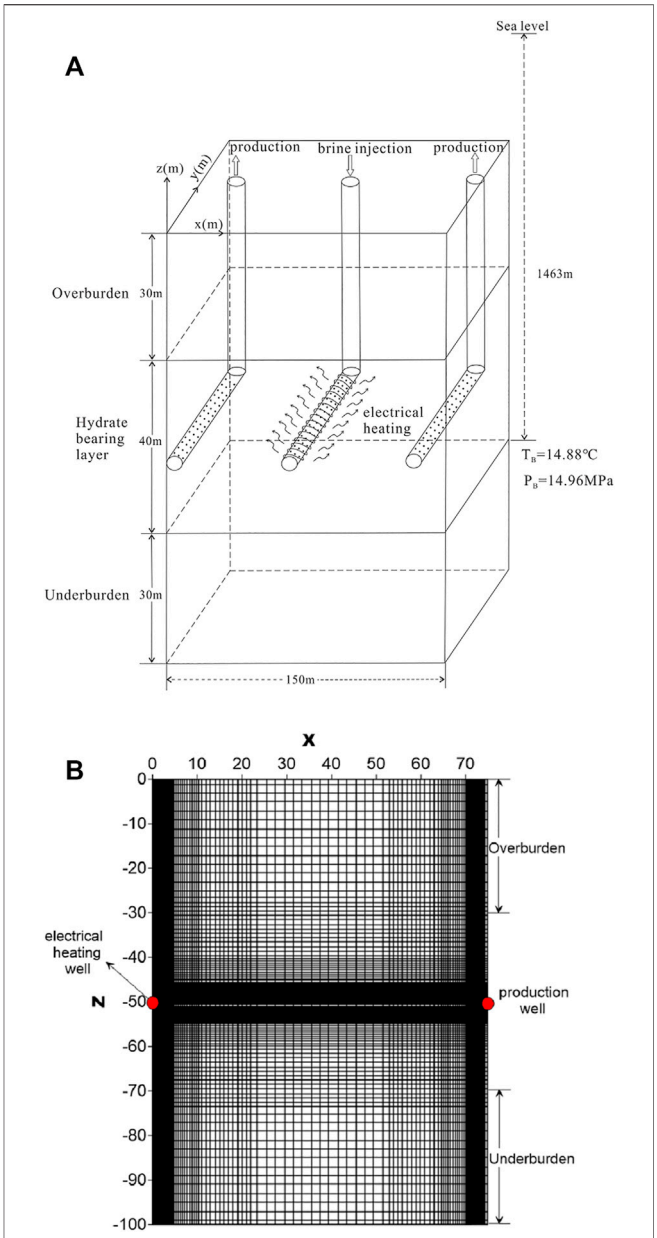

FIGURE 2 | Schematic diagrams of **(A)** the conceptual model and the well configuration and **(B)** domain discretization mesh used in our numerical simulations. The outside of the middle well is surrounded by the electric resistance wire which can release heat when current flows by.

TABLE 1 | Reference hydrate deposit properties and parameters in simulations.

Parameter	Value
The thickness of water-bearing stratums (m)	30
The thickness of the HBL (m)	40
Initial water and hydrate saturation of the HBL (S_A, S_H)	$S_A = 0.6$, $S_H = 0.4$
Gas composition	100% CH_4
Porosity of all layers	0.38
Permeability of all layers (mD)	10
The depth of the base of the HBL (m)	1,463
The average density of sea water (kg/m^3)	1,035
Initial pressure of the base of the HBL (MPa)	14.96
Initial temperature of the base of the HBL (°C)	14.88
Geothermal gradient (°C/m)	0.047
Pore water salinity (mass fraction)	0.03
Grain density of all layers (kg/m^3)	2,600
Compression coefficient of all layers (Pa^{-1})	1.0×10^{-8}
Wet formation thermal conductivity of all layers (W/m/°C)	3.1
Dry formation thermal conductivity of all layers (W/m/°C)	1.0
Rock grain specific heat of all layers (J/kg/°C)	1,000
Relative permeability model of liquid and gas phases (K_{rA}, K_{rG}) Moridis (2014)	$K_{rA} = [(S_A - S_{irA})/(1 - S_{irA})]^n, K_{rG} = [(S_G - S_{irG})/(1 - S_{irA})]^{n_G}$
n (index for aqueous phase)	5
n_G (index for gas phase)	3.5
S_{irA} (irreducible aqueous saturation)	0.30
S_{irG} (irreducible gas saturation)	0.03
Capillary pressure model (P_{cap}) Vangenuchten (1980)	$P_{cap} = -P_0[(S^*)^{-1/\lambda} - 1]^{1-\lambda}, S^* = (S_A - S_{irA})/(S_{mxA} - S_{irA})$
S_{mxA} (maximal aqueous saturation)	1
λ (index for pore structure)	0.45
P_0 (Pa) (the entry capillary pressure)	1.0×10^5

A unit width (1 m) in y direction is used without considering the pressure and temperature drop in the wellbore of the horizontal wells. In addition, a mild well spacing of 75 m is adopted, considering that small well spacing controls less reserves and big well spacing may go beyond the influence radius of the injected electrical heat (Jin et al., 2016). In addition, due to symmetric well configuration, only half of the hydrate deposits need to be simulated. Therefore, the size of the 2D numerical model is 75 m × 100 m in x and z directions, which is discretized into 101 × 114 = 11,514 grid blocks (**Figure 2B**). Because the vicinity of the wellbore had been shown to be critically important to production (Moridis et al., 2009b), a very fine discretization of 0.25 m was used around the horizontal wells. In addition, the spacing intervals increase with the distance to wells, which reaches a size of 2 m at the middle between the wells and at the top and bottom of the model.

The numerical simulator used for the simulation of the behavior of hydrate-bearing geologic systems in this study is TOUGH + HYDRATE, which was developed by the Lawrence Berkeley National Laboratory (Moridis, 2014). The initial distributions of pressure and temperature are, respectively, obtained by hydrostatic pressure distribution and a geothermal gradient of 0.047°C/m (Moridis et al., 2007; Su et al., 2012b). In addition, the base of the HBL initially lies in the hydrate equilibrium condition. As for boundary conditions, constant temperature and pressure boundary are applied to the top and the bottom of the model, and non-flow boundary is applied at x = 0 and x = 75 m during the whole exploitation period (Su et al., 2012a, 2012b; Li et al., 2013).

Simulation Scenarios

The factors that are related to gas production performance of a hydrate deposit can be divided into two classes: formation conditions and artificial operations. The most related formation condition is the permeability of the HBL, which can be improved by hydraulic fracturing, but not involved in our research. Therefore, we mainly consider optimizing artificial operations to promote the exploitation of the NGH, including electrical heating time and power and brine injection pressure, whose effects to gas production are investigated by different exploitation scenarios listed in **Table 2**. As the base case, A0 adopts a brine injection pressure of 17 MPa, which corresponds to the maximum of the wellbore pressure to avoid the overpressure of the HBL (Li et al., 2011). In addition, 2,000 W of electrical heating is applied to the same 2D-simulated hydrate deposit of 75 m × 100 m. In addition, the only depressurization method D1 is also included to verify the feasibility of the new exploitation method of combined brine flooding with electrical heating–assisted depressurization. The production pressures of all scenarios are set to be 8 MPa, which is larger than the pressure at the quadruple point to eliminate the possibility of ice formation.

The following criteria are used to compare the gas production performance of different exploitation scenarios: volumetric rate of total produced methane from wells (Q_P) and volumetric rate of produced methane in gas phase (Q_{PG}), volumetric rate of released methane by hydrate dissociation (Q_R), and volumetric rate of produced water (Q_W); cumulative volume of methane and water produced from wells (V_P and V_W, respectively), gas-to-water ratio (R_{GW}); energy efficiency ratio (η) and net energy gain (E_{net}).

TABLE 2 | Summary of simulation scenarios and part of the simulation results.

Run	Description	P_{pro} (MPa)	P_{inj} (MPa)	P_{ele} (W)	S_R	R_{GW}	η	V_P ($10^8 m^3$)	E_{net} (10^{15}J)
A0	Base case	8	17	2,000	1	6.32	2.33	1.37	2.93
A1	Sensitivity of electrical heating time	8	17	2,000	**0.5**	4.98	5.25	1.09	3.32
A2		8	17	2,000	**0.7**	6.05	3.86	1.30	3.62
B1	Sensitivity of electrical heating power	8	17	**1,000**	0.7	5.21	4.64	1.14	3.37
B2		8	17	**3,000**	0.7	6.38	3.31	1.37	3.61
C1	Sensitivity of brine injection pressure	8	**15**	2,000	0.7	4.54	2.40	1.03	2.25
C2		8	**19**	2,000	0.7	6.43	4.27	1.35	3.90
D1	Only depressurization	8	—	—	—	2.20	5.65	0.97	3.00

Note: P_{pro} is production pressure, P_{inj} is brine injection pressure, P_{ele} is electrical heating power, S_R is the rate of the dissociated hydrate to the initial hydrate when electrical heating stops, and S_R = 1 means electrical heating lasts until the end of simulation. All values in bold denote the investigated parameters needed to be optimized. Part of the simulation results are also given in order to make a comparison of different scenarios, including the gas-to-water ratio (R_{GW}), energy efficiency ratio (η), the cumulative volume of produced methane (V_P), and the net energy gain (E_{net}).

Among these criteria, four of them are particularly important, which can also be classified as relative criterion (R_{GW} and η) and absolute criterion (V_P and E_{net}), which are also listed in **Table 2**. R_{GW} is defined as the ratio of V_P and V_W, while η is the ratio of the recovered energy to the total consumed energy, which can be defined as

$$\boldsymbol{\eta} = \boldsymbol{n} \cdot \Delta \boldsymbol{H_c} \,/\, (\boldsymbol{W} + \boldsymbol{Q}), \tag{1}$$

where ΔH_c is the combustion enthalpy of methane (1 atm, 25°C, 889.6 kJ/mol); n is the amount of substance of the produced methane (mol); W is the energy used for pumping the produced fluids to the ground (kJ); and Q is the total electrical energy injected into the reservoir (kJ). High R_{GW} and η, respectively, indicate satisfying production efficiency and economic performance. Other than the relative criterion, the potential of a specific exploitation scenario can also be validated by a large V_P and E_{net} in the sense of absolute criteria. E_{net} is the difference of the recovered energy with consumed energy calculated as follows:

$$\boldsymbol{E_{net}} = \boldsymbol{n} \cdot \Delta \boldsymbol{H_c} \cdot \left(1 - 1/\boldsymbol{\eta}\right). \tag{2}$$

In order to simulate actual exploitation conditions, all of these criteria are scaled according to the length of the horizontal wells (1,000 m).

RESULTS AND DISCUSSION

Effects of Combined Brine Flooding With Electrical Heating

The exploitation scenario of pure depressurization is first simulated and evaluated, whose methane volumetric rate and water production are shown in **Figure 3**. As shown in **Figure 3A**, the hydrate is rapidly dissociated by depressurization in the initial stage due to the largest pressure difference between production wells and formation, known as pressure driving force. Therefore, Q_R and Q_P, respectively, reach a maximum of 260,000 m^3/day and 43,000 m^3/day in a short time. In addition, Q_R is larger than Q_P in the first 580 days, indicating that the released methane cannot be produced in time due to the low permeability of the HBL. With the reduction of pressure driving force and exhaustion of the hydrate around production wells, Q_R rapidly drops below Q_P, and the remaining methane is discharged from production wells. Then, Q_P and Q_R almost keep stable before a sudden decrease happening at 5 years. The reason is that the hydrate between the HBL and surrounding permeable water-bearing stratums is completely dissociated, resulting in rapid water invasion, proven by the sudden increase of the water-produced rate (Q_W) at 5 years in **Figure 3B**. Massive water production slows down the propagation of low pressure. Therefore, Q_P and Q_R keep decreasing with a similar trend and reach a value of 6,500 m^3/day at the end of simulation, which is much lower than the commercially viable production rate.

However, Q_W keeps increasing in the whole simulation process due to increase of formation permeability after hydrate dissociation and the influence of permeable water-bearing stratums. The different variations of Q_P and Q_W indicate that gas production is controlled by methane from hydrate dissociation rather than original methane dissolved in *in situ* water. In addition, the released methane can be produced in free gas or in dissolution. Initially, due to rapid release of methane from hydrate dissociation, free gas takes a large proportion of the total produced methane. However, Q_G gradually decreases with reduction of Q_R and becomes zero at 2,650 days, indicating that methane is produced completely in dissolution after then. The relative criterion (R_{GW} and η) and absolute criterion (V_P and E_{net}) to judge gas production performance are given in **Figure 4**. At the end of the simulation, the cumulative volume of the produced methane for only depressurization is 9.7×10^7 m^3, corresponding to an average production rate of 13,275 m^3/day. With the increase of the produced water rate and the decrease of produced methane rate, R_{GW} and η of only depressurization keeps descending, respectively, with a final value of 2.20 and 5.65.

From the previous analysis, only depressurization is inefficient for the challenging hydrate deposit with permeable overlying and underlying layers. The hydrate dissociation rate and methane production rate will rapidly decrease when the water from the surrounding permeable layers invades into the HBL. Therefore, thermal stimulation by combined brine flooding with electrical heating is conducted after 5 years of only depressurization in order to promote hydrate dissociation. For the base case, brine injection (20°C) at a constant pressure of 17 MPa and electrical

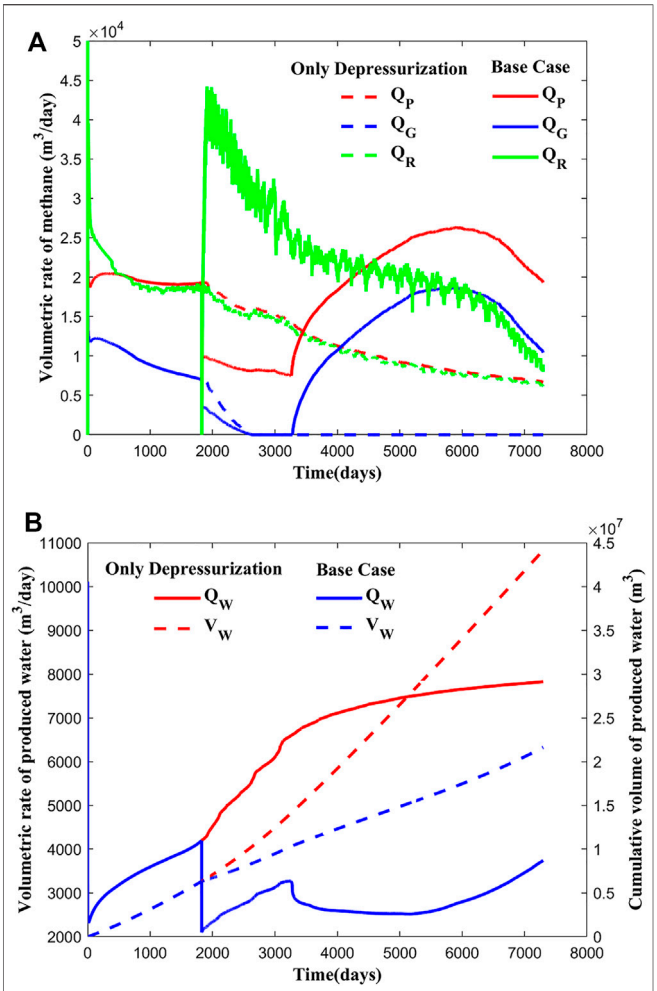

FIGURE 3 | Evolution of **(A)** methane production rate (Q_P), methane production rate in gaseous phase (Q_{PG}) and release rate (Q_R), **(B)** water production rate (Q_W) and water production volume (V_W) for the only depressurization method and combined brine flooding with electrical heating–assisted depressurization method (the base-case). The unit of the volumetric rate is measured at standard temperature and pressure.

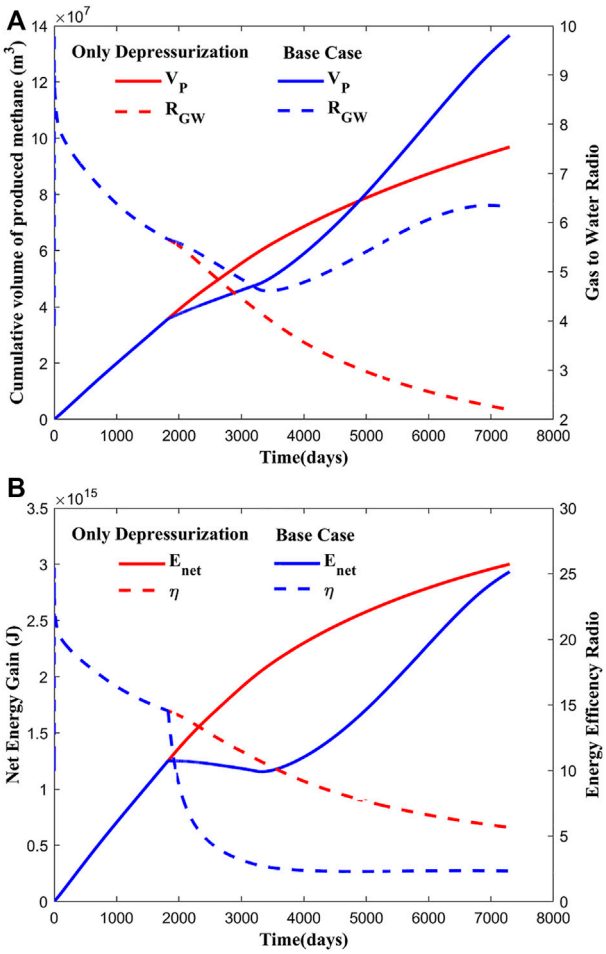

FIGURE 4 | Evolution of **(A)** methane production volume (V_P) and gas-to-water ratio (R_{GW}), **(B)** energy efficiency ratio (η) and net energy gain (E_{net}) for the only depressurization method and combined brine flooding with electrical heating–assisted depressurization method (the base-case).

heating with a power of 2,000 W are simultaneously applied to the left well, while the other well is still used for depressurization at a constant pressure of 8 MPa. For comparison with only depressurization, methane production, water production, and energy gain of the base case are also given in **Figures 3**, **4**. In addition, **Figures 5–8**, respectively, show the evolution of temperature (T), hydrate saturation (S_H), gas saturation (S_G) and salinity (X_{inh}) of the base case in order to figure out the variation of the system state over time under thermal stimulation.

When thermal stimulation starts at 5 years, Q_R of the base case rapidly increases and reaches a peak of 45,000 m^3/day, proving that hydrate dissociation is accelerated by the electrical heat, which is carried by the brine into the deep of the HBL. On the other hand, the vacated pore space after hydrate dissociation increases the permeability of formation, which is beneficial to the flow of the heated brine. As a result, hydrate complete dissociation area and high-temperature region around the injection well move rapidly toward the production well (**Figures 5**, **6**). Contrary to the immediate increase of Q_R, Q_P and Q_{PG} first drop by half after thermal stimulation due to the halving of production wells and then keep decreasing until 3,280 days. During this stage, the released methane is detained in the HBL due to the distance between the wells, which leads to the increase of gas saturation (**Figures 7A,B**). Therefore, further dissociation of the hydrate is suppressed, and Q_R gradually decreases.

When the released methane reaches the production well at 3,280 days (**Figure 7C**), Q_P and Q_G start rapidly increasing, which is 1,455 days later than the increase of Q_R. Then, Q_P exceeds Q_R at 4,420 days and reaches a peak of 6,140 m^3/day at around 6,000 days, indicating that the detained methane is gradually produced. After 6,000 days, a quick drop of Q_R (as well as Q_P and Q_{PG}) appears due to the exhaustion of the hydrate, validated by the small green part in **Figures 6E,F**. In addition, the similar variation between Q_P and Q_{PG} indicates that gaseous methane makes the main contribution of the increase of Q_P after

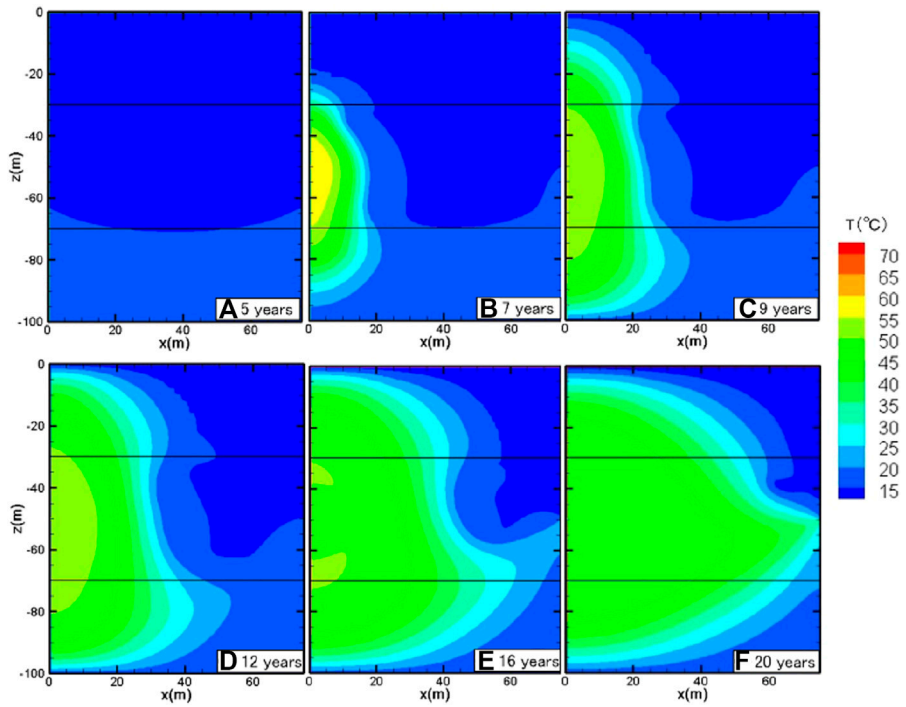

FIGURE 5 | Evolution of spatial distributions of temperature (T) over time: **(A)** 5 years, **(B)** 7 years, **(C)** 9 years, **(D)** 12 years, **(E)** 16 years, and **(F)** 20 years for the combined brine flooding with electrical heating–assisted depressurization method (the base-case).

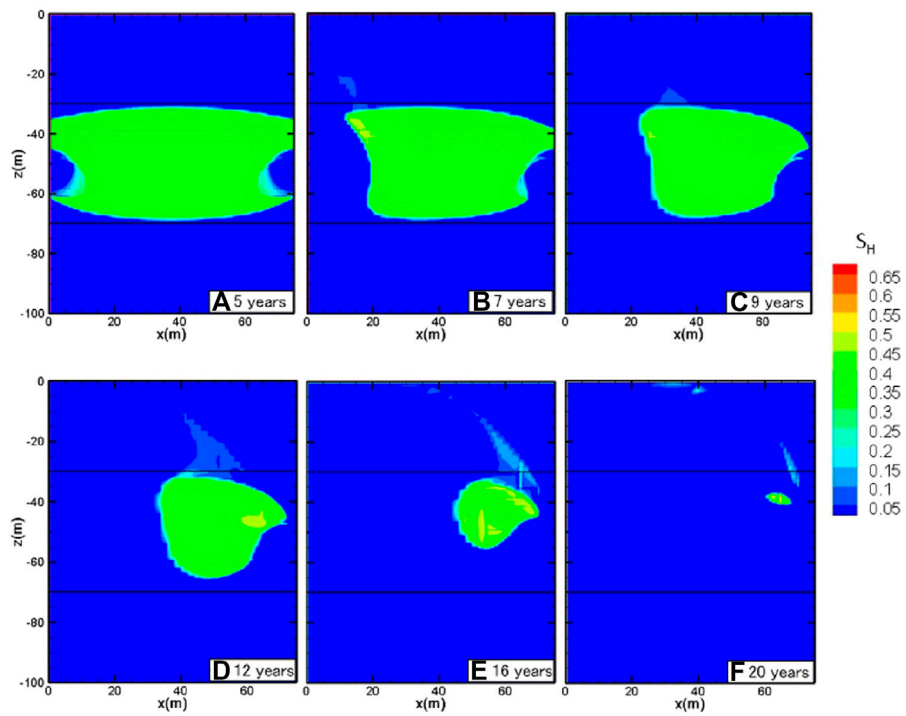

FIGURE 6 | Evolution of spatial distributions of hydrate saturation (S_H) over time: **(A)** 5 years, **(B)** 7 years, **(C)** 9 years, **(D)** 12 years, **(E)** 16 years, and **(F)** 20 years for the combined brine flooding with electrical heating–assisted depressurization method (the base-case).

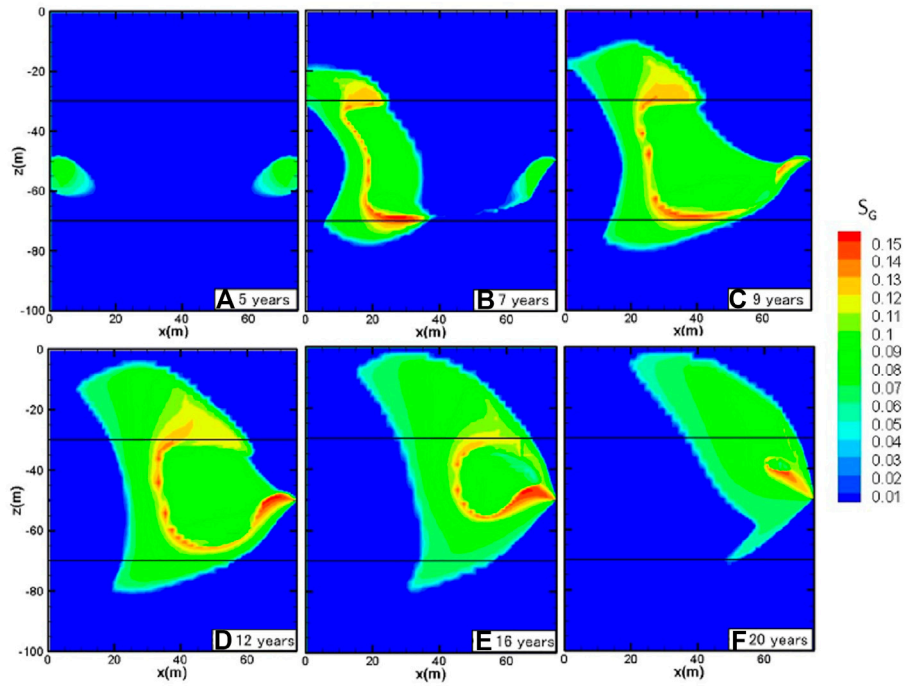

FIGURE 7 | Evolution of spatial distributions of gas saturation (S_G) over time: **(A)** 5 years, **(B)** 7 years, **(C)** 9 years, **(D)** 12 years, **(E)** 16 years, and **(F)** 20 years for the combined brine flooding with electrical heating–assisted depressurization method (the base-case).

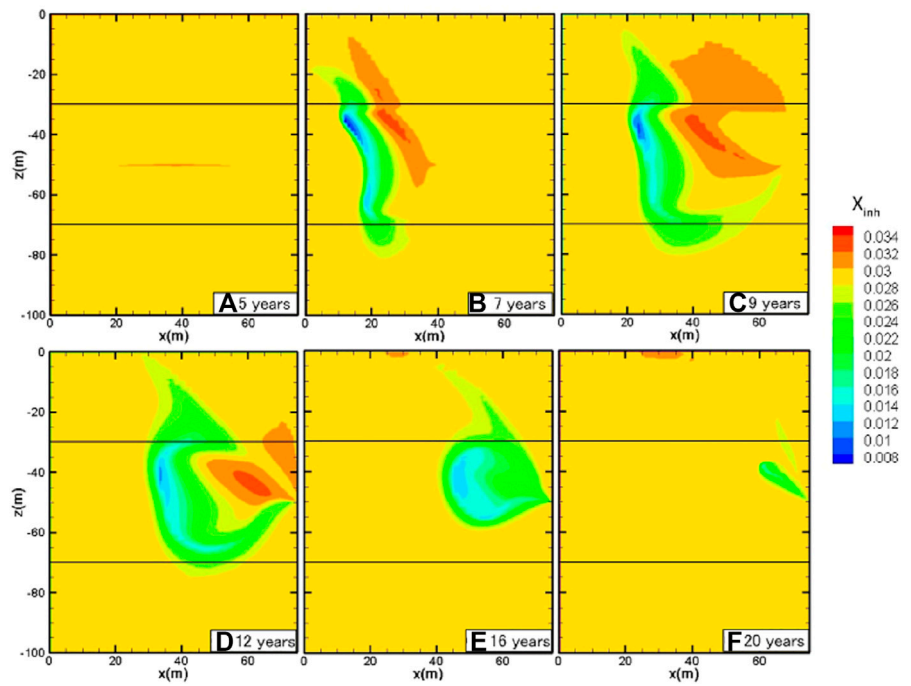

FIGURE 8 | Evolution of spatial distributions of salinity (X_{inh}) over time: **(A)** 5 years, **(B)** 7 years, **(C)** 9 years, (D) 12 years, **(E)** 16 years, and **(F)** 20 years for the combined brine flooding with electrical heating–assisted depressurization method (the base-case).

thermal stimulation. As shown in **Figure 8**, a high salinity abnormal forms at the behind of the dissociation interfaces around the injection well. This is a sign of secondary hydrate formation because that salt is excluded from the lattice of the hydrate, which originates from the pressure increment by brine injection and should be responsible for the fluctuations of Q_R after thermal stimulation. With the exhaustion of the hydrate, the high salinity abnormal gradually disappears.

Different from the continuous increase of the water production rate of only depressurization, water production of the base case is suppressed when the released methane reaches the production well, because the relative permeability of water is inversely proportional to gas saturation. With the discharge of methane and increase of absolute permeability of formation, Q_W increases again after 5,500 days but is still much lower than that of only depressurization. From **Figure 4A**, thermal stimulation by combined brine flooding with electrical heating can greatly increase methane recovery, with a higher V_P (except the period before methane reaches production well) and R_{GW} over only depressurization. At the end of the simulation, the cumulative volume of the produced methane is increased by 41% with thermal stimulation. However, the net energy gain of the base case shows no improvement over only depressurization because the additional methane recovery is offset by massive injected electrical heat, and a rather low energy efficiency ratio of 2.33 is obtained by thermal stimulation. Therefore, the energy efficiency of the combined brine flooding with electrical heating–assisted depressurization needs to be improved before field application.

Sensitivity Analysis of Electrical Heating Time

In order to save energy and gain a higher energy efficiency, electrical heating should be terminated at the later stage of the base case because there is only little hydrate left (**Figures 6E,F**). Therefore, another two runs of A1 and A2 are conducted to determine the effects of the electrical heating time, which, respectively, terminate electrical heating when the rate of the dissociated hydrate to the initial hydrate (S_R) reaches 0.5 (at 3,156 days) and 0.7 (at 4,579 days). The base case corresponds to an S_R of 1.0, which means that electrical heating lasts until the end of the simulation. Though electrical heating stops at an earlier time for A1 and A2, brine of 20°C is still injected into the HBL with an injection pressure of 17 MPa to assist the drainage of methane. As shown in **Figure 9A**, longer electrical heating time leads to a higher Q_P due to more hydrate dissociation. In addition, the termination of electrical heating results in the increase of Q_W on account of the alleviation of water production restriction by the reduction of gas saturation around the production well (**Figure 9B**). However, Q_W increases with increasing of S_R at the end of the simulation because more vacated pore space for a longer electrical heating time leads to higher formation permeability. In addition, the final V_W is almost equal for different electrical heating times.

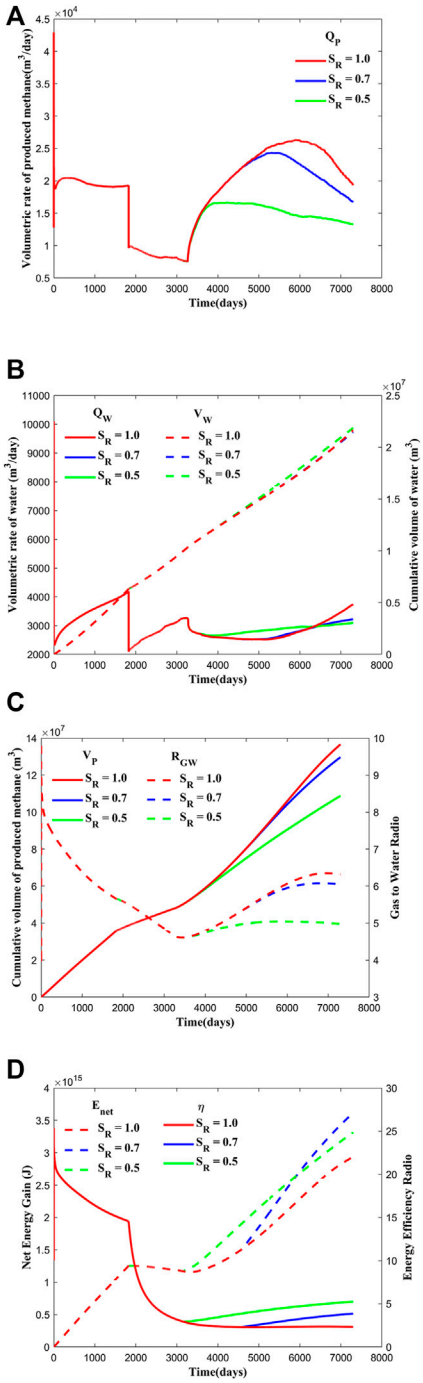

FIGURE 9 | Evolution of **(A)** methane production rate (Q_P), **(B)** water production rate (Q_W) and water production volume (V_W), **(C)** methane production volume (V_P) and gas-to-water ratio (R_{GW}), and **(D)** energy efficiency ratio (η) and net energy gain (E_{net}) under different electrical heating times.

The optimization of electrical heating time can be achieved by the criteria shown in **Figures 9C,D**. Compared with the base case, V_P only decreases by 5.1%, but the injected heat is reduced by 49.7% for terminating electrical heating when 70% hydrate has already been dissociated (SR = 0.7). Therefore, the energy

efficiency and net energy gain can be greatly improved by decreasing electrical heating time. However, further advancing the termination of electrical heating with an S_R of 0.5 decreases V_P by 16.1%, and the net energy gain is lower than that of terminating electrical heating with an S_R of 0.7, indicating that stopping electrical heating prematurely is disadvantageous to methane production due to insufficient hydrate dissociation, even though a higher energy efficiency ratio is obtained. Therefore, a medium electrical heating time is preferred for gas production from hydrate deposit in order to accelerate hydrate dissociation and gain satisfactory energy efficiency. Thus, the subsequent simulations all terminate electrical heating when 70% of hydrate is dissociated in order to avoid massive energy waste.

Sensitivity Analysis of Electrical Heating Power

Apparently, the gas production performance of the combined brine flooding with electrical heating–assisted depressurization is closely related to electrical heating power. Therefore, another two simulations with a power of 1,000 W (B1) and 3,000 W (B2) are conducted to explore the effects of electrical heating power. The two additional simulations adopt same parameters as A2 except the electrical heating power, which also terminate electrical heating when 70% hydrate has already been dissociated in order to save energy. As shown in **Figure 10A**, Q_P initially increases with electrical heating power because of the accelerated hydrate dissociation. Moreover, a larger power not only induces earlier increase of Q_P due to advanced breakthrough of released methane from the injection well to the production well but also induces earlier drop of Q_P due to the advanced termination of electrical heating. In addition, faster exhaustion of the hydrate induces that Q_P decreases with increasing of the electrical heating power at the end of the simulation. Contrary to Q_P, a larger power leads to a lower Q_W at an early time and a higher Q_W at a later time (**Figure 10B**). The different variation of methane production and water production is reasonable considering that the relative permeability of gas phase and aqueous phase change oppositely at all times. In addition, the final V_W is basically unchanged with electrical heating power.

The relative criteria and absolute criteria are also given in **Figures 10C,D** in order to optimize the electrical heating power. From **Figure 10C**, V_P and R_{GW} increase with the electrical heating power though with a decreasing rate. Compared with the electrical heating power of 2,000 W, V_P increases by 5.9% for the electrical heating power of 3,000 W, while V_P decreases by 12.0% for the electrical heating power of 1,000 W. Thus, a low electrical heating power of 1,000 W is inefficient for gas production from the hydrate deposit though with a high energy efficiency ratio (**Figure 10D**). In addition, the net energy gain of 2,000 and 3,000 W is basically the same, indicating that the additional recovered methane just catches up with the enlarged electrical heat injection. At the same time, increasing electrical heating power also enlarges the risks of wellbore failure due to thermal stress variation. Therefore, a mild electrical heating power is preferred for increasing methane recovery and reducing geological risks.

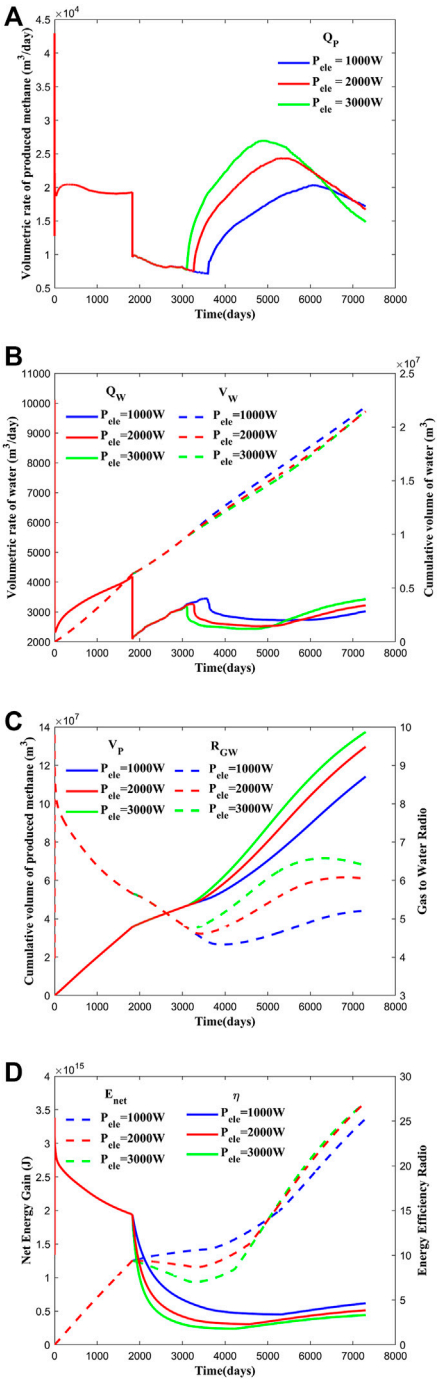

FIGURE 10 | Evolution of **(A)** methane production rate (Q_P), **(B)** water production rate (Q_W) and water production volume (V_W) under different electrical heating powers, **(C)** methane production volume (V_P) and gas-to-water ratio (R_{GW}), and **(D)** energy efficiency ratio (η) and net energy gain (E_{net}) under different electrical heating powers.

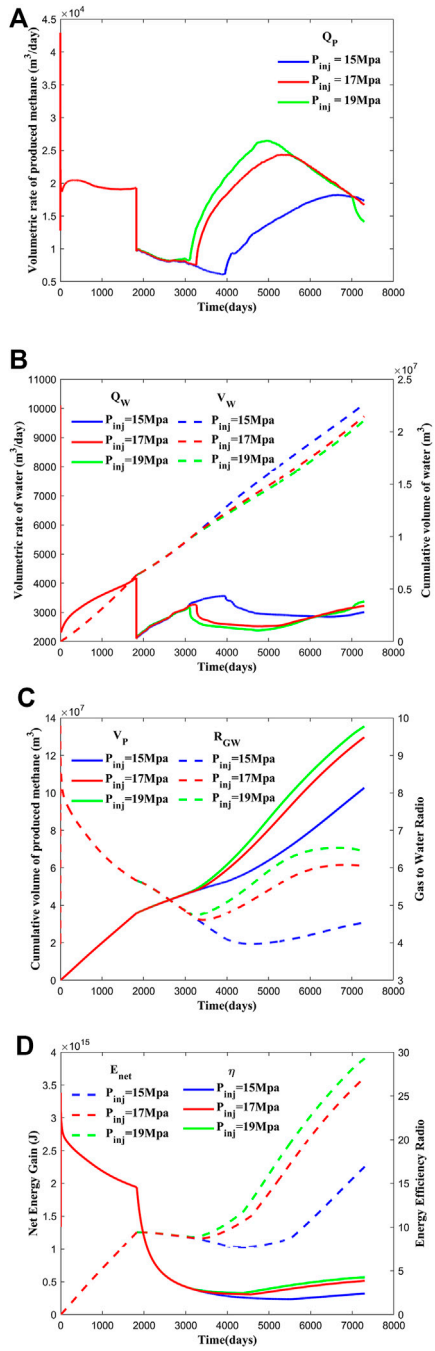

FIGURE 11 | Evolution of **(A)** methane production rate (Q_P), **(B)** water production rate (Q_W) and water production volume (V_W), **(C)** methane production volume (V_P) and gas-to-water ratio (R_{GW}), and **(D)** energy efficiency ratio (η) and net energy gain (E_{net}) under different brine injection pressures.

Sensitivity Analysis of Brine Injection Pressure

Other than electrical heating power, brine injection pressure is also a key parameter related to gas production performance, whose effects are determined by another two procedures with injection pressure of 15 MPa (C1) and 19 MPa (C2). Except brine injection pressure, other parameters of C1 and C2 are the same as A2. From the simulation results of methane and water production shown in **Figures 11A,B**, Q_P initially increases with injection pressure because of faster brine injection, leading to a larger heat diffusion rate. Driven by larger pressure gradient between wells, faster breakthrough of released methane is also realized by higher injection pressure. At the same time, the advanced termination of electrical heating after 70% of hydrate dissociation for higher injection pressure induces an earlier drop and a lower final value of Q_P. As clarified before, Q_W still varies oppositely with Q_P. However, a confusing phenomenon of water production is that larger injection pressure, instead, possesses a lower final V_W. This can be explained as more methane accumulation around the production well by higher injection pressure results in a stronger suppression of water production in the early stage of the thermal stimulation.

The superiority of higher brine injection pressure is adequately verified by higher methane recovery and gas-to-water ratio (**Figure 11C**), as well as the higher energy efficiency ratio and net energy gain (**Figure 11D**). Raising brine injection pressure from 15 to 17 MPa increases E_{net} by 60.4%, while further raising injection pressure to 19 MPa only increases E_{net} by 8.0%. On the other hand, higher injection pressure also enlarges the risks of geological hazards, such as reservoir instability and submarine landslide. Therefore, the selection of brine injection pressure should be carefully and comprehensively considered regarding the factors of gas production and geological risks.

CONCLUSION

This study numerically verifies the feasibility of combined brine flooding with electrical heating–assisted depressurization in horizontal wells to improve gas production from the natural gas hydrate in the Shenhu area of the South China Sea. By analyzing the simulation results of methane recovery, water production, and energy gain, the optimizations of electrical heating time and power and brine injection pressure are achieved, and the following conclusions can be drawn:

Thermal stimulation by combined brine flooding with electrical heating can greatly improve methane recovery. After 20 years of production, the cumulative methane production of combined brine injection with electrical heating–assisted depressurization is 1.41 times of that conducted by the only depressurization method. However, the rather low energy efficiency ratio of the thermal stimulation method results in a similar net energy gain with the only depressurization method.

In order to improve energy efficiency, the advanced termination of electrical heating is proposed and numerically evaluated. The simulation results of three different termination times indicate that stopping electrical heating prematurely is disadvantageous to methane production due to insufficient hydrate dissociation. At the same time, keeping on electrical heating after 70% of hydrate dissociation results in massive energy wastes. Therefore, a medium electrical heating time is preferred for gas production from the hydrate deposit, whose superiority is proven by the largest net energy gain and a satisfactory energy efficiency ratio.

Increasing electrical heating power and brine injection pressure leads to better exploitation performance with higher methane recovery and net energy gain. However, the degree of improvement is gradually weakened after a certain threshold; in the meantime, the risks of wellbore and reservoir failures increase with these factors. Therefore, the selection of electrical heating power and injection pressure should be performed carefully and comprehensively, considering both the efficiency of the gas recovery and the risks of geological hazard.

This study only optimized the artificial operations of the tripartite exploitation strategy, however, the effect of reservoir physical property, hydrate saturation, and fluid component on the gas recovery has not yet been well-revealed and will be our next stage of investigation. In addition, comprehensive comparison with other electrical heating methods, for example, low-frequency electrical heating and electromagnetic heating, remains to be conducted.

DATA AVAILABILITY STATEMENT

The raw data supporting the conclusion of this article will be made available by the authors, without undue reservation.

AUTHOR CONTRIBUTIONS

QZ: conceptualization, methodology, data curation, visualization, and writing—original draft. YW: conceptualization, methodology, visualization, writing—review and editing, and supervision.

FUNDING

The research is supported by the Original Innovation Research Program of the Chinese Academy of Sciences (CAS) under Grant number ZDBS-LY-DQC003, and the Key Research Program of the Institute of Geology and Geophysics, CAS under Grant numbers IGGCAS-2019031 and SZJJ-201901.

ACKNOWLEDGMENTS

We are grateful to editors and reviewers for important questions and suggestions.

REFERENCES

Boswell, R., and Collett, T. S. (2011). Current Perspectives on Gas Hydrate Resources. *Energy Environ. Sci.* 4 (4), 1206–1215. doi:10.1039/c0ee00203h

Chong, Z. R., Yang, S. H. B., Babu, P., Linga, P., and Li, X.-S. (2016). Review of Natural Gas Hydrates as an Energy Resource: Prospects and Challenges. *Appl. Energ.* 162, 1633–1652. doi:10.1016/j.apenergy.2014.12.061

Chong, Z. R., Yin, Z., Tan, J. H. C., and Linga, P. (2017). Experimental Investigations on Energy Recovery from Water-Saturated Hydrate Bearing Sediments via Depressurization Approach. *Appl. Energ.* 204, 1513–1525. doi:10.1016/j.apenergy.2017.04.031

Collett, T. S. (2002). Energy Resource Potential of Natural Gas Hydrates. *AAPG Bull.* 86 (11), 1971–1992. doi:10.1306/61eeddd2-173e-11d7-8645000102c1865d

Falser, S., Uchida, S., Palmer, A. C., Soga, K., and Tan, T. S. (2012). Increased Gas Production from Hydrates by Combining Depressurization with Heating of the Wellbore. *Energy Fuels* 26 (10), 6259–6267. doi:10.1021/ef3010652

Feng, J.-C., Li, G., Li, X.-S., Li, B., and Chen, Z.-Y. (2013). Evolution of Hydrate Dissociation by Warm Brine Stimulation Combined Depressurization in the South China Sea. *Energies* 6 (10), 5402–5425. doi:10.3390/en6105402

Feng, J.-C., Li, X.-S., Li, G., Li, B., Chen, Z.-Y., and Wang, Y. (2014). Numerical Investigation of Hydrate Dissociation Performance in the South China Sea with Different Horizontal Well Configurations. *Energies* 7 (8), 4813–4834. doi:10.3390/en7084813

Feng, J.-C., Wang, Y., Li, X.-S., Li, G., Zhang, Y., and Chen, Z.-Y. (2015). Effect of Horizontal and Vertical Well Patterns on Methane Hydrate Dissociation Behaviors in Pilot-Scale Hydrate Simulator. *Appl. Energ.* 145, 69–79. doi:10.1016/j.apenergy.2015.01.137

He, J., Li, X., Chen, Z., Li, Q., Zhang, Y., Wang, Y., et al. (2021). Combined Styles of Depressurization and Electrical Heating for Methane Hydrate Production. *Appl. Energ.* 282, 116112. doi:10.1016/j.apenergy.2020.116112

Jin, G., Xu, T., Xin, X., Wei, M., and Liu, C. (2016). Numerical Evaluation of the Methane Production from Unconfined Gas Hydrate-Bearing Sediment by thermal Stimulation and Depressurization in Shenhu Area, South China Sea. *J. Nat. Gas Sci. Eng.* 33, 497–508. doi:10.1016/j.jngse.2016.05.047

Koh, C. A., Sum, A. K., and Sloan, E. D. (2012). State of the Art: Natural Gas Hydrates as a Natural Resource. *J. Nat. Gas Sci. Eng.* 8, 132–138. doi:10.1016/j.jngse.2012.01.005

Koh, D.-Y., Kang, H., Lee, J.-W., Park, Y., Kim, S.-J., Lee, J., et al. (2016). Energy-Efficient Natural Gas Hydrate Production Using Gas Exchange. *Appl. Energ.* 162, 114–130. doi:10.1016/j.apenergy.2015.10.082

Koh, C. A. (2002). Towards a Fundamental Understanding of Natural Gas Hydrates. *Chem. Soc. Rev.* 31 (3), 157–167. doi:10.1039/b008672j

Konno, Y., Masuda, Y., Akamine, K., Naiki, M., and Nagao, J. (2016). Sustainable Gas Production from Methane Hydrate Reservoirs by the Cyclic Depressurization Method. *Energ. Convers. Manage.* 108, 439–445. doi:10.1016/j.enconman.2015.11.030

Li, G., Moridis, G. J., Zhang, K., and Li, X.-S. (2010). Evaluation of Gas Production Potential from Marine Gas Hydrate Deposits in Shenhu Area of South China Sea. *Energy Fuels* 24 (11), 6018–6033. doi:10.1021/ef100930m

Li, G., Moridis, G. J., Zhang, K., and Li, X.-s. (2011). The Use of Huff and Puff Method in a Single Horizontal Well in Gas Production from marine Gas Hydrate Deposits in the Shenhu Area of South China Sea. *J. Pet. Sci. Eng.* 77 (1), 49–68. doi:10.1016/j.petrol.2011.02.009

Li, G., Li, X.-S., Zhang, K., Li, B., and Zhang, Y. (2013). Effects of Impermeable Boundaries on Gas Production from Hydrate Accumulations in the Shenhu Area of the South China Sea. *Energies* 6 (8), 4078–4096. doi:10.3390/en6084078

Li, B., Liu, S.-D., Liang, Y.-P., and Liu, H. (2018a). The Use of Electrical Heating for the Enhancement of Gas Recovery from Methane Hydrate in Porous media. *Appl. Energ.* 227, 694–702. doi:10.1016/j.apenergy.2017.08.066

Li, J.-F., Ye, J. L., Ye, J.-L., Qin, X.-W., Qiu, H.-J., Wu, N.-Y., et al. (2018b). The First Offshore Natural Gas Hydrate Production Test in South China Sea. *China Geol.* 1 (1), 5–16. doi:10.31035/cg2018003

Li, L., Li, X., Wang, Y., Luo, Y., and Li, B. (2020). Analyzing the Applicability of *In Situ* Heating Methods in the Gas Production from Natural Gas Hydrate-Bearing Sediment with Field Scale Numerical Study. *Energ. Rep.* 6, 3291–3302. doi:10.1016/j.egyr.2020.11.208

Liang, Y.-P., Liu, S., Wan, Q.-C., Li, B., Liu, H., and Han, X. (2018). Comparison and Optimization of Methane Hydrate Production Process Using Different Methods in a Single Vertical Well. *Energies* 12 (1), 124. doi:10.3390/en12010124

Liang, Y., Tan, Y., Luo, Y., Zhang, Y., and Li, B. (2020). Progress and Challenges on Gas Production from Natural Gas Hydrate-Bearing Sediment. *J. Clean. Prod.* 261, 121061. doi:10.1016/j.jclepro.2020.121061

Liu, Y., Hou, J., Chen, Z., Su, H., Zhao, E., and Li, G. (2020). A Novel Natural Gas Hydrate Recovery Approach by Delivering Geothermal Energy through Dumpflooding. *Energ. Convers. Manage.* 209, 112623. doi:10.1016/j.enconman.2020.112623

Liu, S., Li, H., Wang, B., and Sun, B. (2022). Accelerating Gas Production of the Depressurization-Induced Natural Gas Hydrate by Electrical Heating. *J. Pet. Sci. Eng.* 208, 109735. doi:10.1016/j.petrol.2021.109735

Minagawa, H., Ito, T., Kimura, S., Kaneko, H., Noda, S., and Tenma, N. (2018). Depressurization and Electrical Heating of Methane Hydrate Sediment for Gas Production: Laboratory-Scale Experiments. *J. Nat. Gas Sci. Eng.* 50, 147–156. doi:10.1016/j.jngse.2017.10.024

Mokheimer, E. M. A., Hamdy, M., Abubakar, Z., Shakeel, M. R., Habib, M. A., and Mahmoud, M. (2019). A Comprehensive Review of Thermal Enhanced Oil Recovery: Techniques Evaluation. *J. Energ. Resour. Technol.-Trans. ASME* 141 (3), 030801. doi:10.1115/1.4041096

Moridis, G. J., and Reagan, M. T. (2011). Estimating the Upper Limit of Gas Production from Class 2 Hydrate Accumulations in the Permafrost: 1. Concepts, System Description, and the Production Base Case. *J. Pet. Sci. Eng.* 76 (3-4), 194–204. doi:10.1016/j.petrol.2010.11.023

Moridis, G. J., Collett, T. S., Dallimore, S. R., Satoh, T., Hancock, S., and Weatherill, B. (2004). Numerical Studies of Gas Production from Several CH4 Hydrate Zones at the Mallik Site, Mackenzie Delta, Canada. *J. Pet. Sci. Eng.* 43 (3-4), 219–238. doi:10.1016/j.petrol.2004.02.015

Moridis, G. J., Kowalsky, M. B., Pruess, K., and Lab, L. B. N. (2007). Depressurization-induced Gas Production from Class 1 Hydrate Deposits. *SPE Reserv. Eval. Eng.* 10 (5), 458–481. doi:10.2118/97266-Pa

Moridis, G. J., Collett, T. S., Boswell, R., Kurihara, M., Reagan, M. T., Koh, C., et al. (2009a). Toward Production from Gas Hydrates: Current Status, Assessment of Resources, and Simulation-Based Evaluation of Technology and Potential. *SPE Reserv. Eval. Eng.* 12 (5), 745–771. doi:10.2118/114163-Pa

Moridis, G. J., Reagan, M. T., Kim, S.-J., Seol, Y., and Zhang, K. (2009b). Evaluation of the Gas Production Potential of Marine Hydrate Deposits in the Ulleung Basin of the Korean East Sea. *SPE J.* 14 (4), 759–781. doi:10.2118/110859-Pa

Moridis, G. J., Kim, J., Reagan, M. T., and Kim, S.-J. (2013). Feasibility of Gas Production from a Gas Hydrate Accumulation at the UBGH2-6 Site of the Ulleung basin in the Korean East Sea. *J. Pet. Sci. Eng.* 108, 180–210. doi:10.1016/j.petrol.2013.03.002

Moridis, G. J. (2014). "User's Manual for the Hydrate v1.5 Option of TOUGH+V1.5: a Code for the Simulation of System Behavior in Hydrate-Bearing Geologic media," in *Earth Sciences Division* (Berkeley, CA 94720: Lawrence Berkeley National Laboratory).

Oyama, H., Konno, Y., Suzuki, K., and Nagao, J. (2012). Depressurized Dissociation of Methane-Hydrate-Bearing Natural Cores with Low Permeability. *Chem. Eng. Sci.* 68 (1), 595–605. doi:10.1016/j.ces.2011.10.029

Sloan, E. D. (2003). Fundamental Principles and Applications of Natural Gas Hydrates. *Nature* 426 (6964), 353–359. doi:10.1038/nature02135

Su, Z., Cao, Y., Wu, N., and He, Y. (2011). Numerical Analysis on Gas Production Efficiency from Hydrate Deposits by Thermal Stimulation: Application to the Shenhu Area, South China Sea. *Energies* 4 (2), 294–313. doi:10.3390/en4020294

Su, Z., He, Y., Wu, N., Zhang, K., and Moridis, G. J. (2012a). Evaluation on Gas Production Potential from Laminar Hydrate Deposits in Shenhu Area of South China Sea through Depressurization Using Vertical wells. *J. Pet. Sci. Eng.* 86-87, 87–98. doi:10.1016/j.petrol.2012.03.008

Su, Z., Moridis, G. J., Zhang, K., and Wu, N. (2012b). A Huff-And-Puff Production of Gas Hydrate Deposits in Shenhu Area of South China Sea through a Vertical Well. *J. Pet. Sci. Eng.* 86-87, 54–61. doi:10.1016/j.petrol.2012.03.020

Su, Z., Huang, L., Wu, N., and Yang, S. (2013). Effect of thermal Stimulation on Gas Production from Hydrate Deposits in Shenhu Area of the South China Sea. *Sci. China Earth Sci.* 56 (4), 601–610. doi:10.1007/s11430-013-4587-4

Sun, J., Ning, F., Li, S., Zhang, K., Liu, T., Zhang, L., et al. (2015). Numerical Simulation of Gas Production from Hydrate-Bearing Sediments in the Shenhu Area by Depressurising: The Effect of burden Permeability. *J. Unconventional Oil Gas Resour.* 12, 23–33. doi:10.1016/j.juogr.2015.08.003

Sun, Y., Ma, X., Guo, W., Jia, R., and Li, B. (2019). Numerical Simulation of the Short- and Long-Term Production Behavior of the First Offshore Gas Hydrate Production Test in the South China Sea. *J. Pet. Sci. Eng.* 181, 106196. doi:10.1016/j.petrol.2019.106196

Sung, W., Lee, H., Lee, H., and Lee, C. (2002). Numerical Study for Production Performances of a Methane Hydrate Reservoir Stimulated by Inhibitor Injection. *Energ. Sourc.* 24 (6), 499–512. doi:10.1080/00908310290086527

Vangenuchten, M. T. (1980). A Closed-form Equation for Predicting the Hydraulic Conductivity of Unsaturated Soils. *Soil Sci. Soc. Am. J.* 44 (5), 892–898. doi:10.2136/sssaj1980.03615995004400050002x

Wan, Q.-C., Si, H., Li, B., and Li, G. (2018). Heat Transfer Analysis of Methane Hydrate Dissociation by Depressurization and thermal Stimulation. *Int. J. Heat Mass Transfer* 127, 206–217. doi:10.1016/j.ijheatmasstransfer.2018.07.016

Wan, Q.-C., Chen, L.-L., Li, B., Peng, K., and Wu, Y.-Q. (2020a). Insights into the Control Mechanism of Heat Transfer on Methane Hydrate Dissociation via Depressurization and Wellbore Heating. *Ind. Eng. Chem. Res.* 59 (22), 10651–10663. doi:10.1021/acs.iecr.0c00705

Wan, Q.-C., Si, H., Li, B., Yin, Z.-Y., Gao, Q., Liu, S., et al. (2020b). Energy Recovery Enhancement from Gas Hydrate Based on the Optimization of thermal Stimulation Modes and Depressurization. *Appl. Energ.* 278, 115612. doi:10.1016/j.apenergy.2020.115612

Wang, P., Yang, M., Chen, B., Zhao, Y., Zhao, J., and Song, Y. (2017). Methane Hydrate Reformation in Porous media with Methane Migration. *Chem. Eng. Sci.* 168, 344–351. doi:10.1016/j.ces.2017.04.036

Wang, B., Dong, H., Liu, Y., Lv, X., Liu, Y., Zhao, J., et al. (2018). Evaluation of thermal Stimulation on Gas Production from Depressurized Methane Hydrate Deposits☆. *Appl. Energ.* 227, 710–718. doi:10.1016/j.apenergy.2017.08.005

Wang, B., Dong, H., Fan, Z., Liu, S., Lv, X., Li, Q., et al. (2020). Numerical Analysis of Microwave Stimulation for Enhancing Energy Recovery from Depressurized Methane Hydrate Sediments. *Appl. Energ.* 262, 114559. doi:10.1016/j.apenergy.2020.114559

White, M. D., Wurstner, S. K., and McGrail, B. P. (2011). Numerical Studies of Methane Production from Class 1 Gas Hydrate Accumulations Enhanced with Carbon Dioxide Injection. *Mar. Pet. Geology.* 28 (2), 546–560. doi:10.1016/j.marpetgeo.2009.06.008

Wu, S., and Wang, J. (2018). On the China′s Successful Gas Production Test from marine Gas Hydrate Reservoirs. *Chin. Sci. Bull.* 63 (1), 2–8. doi:10.1360/n972017-00645

Wu, N. Y., Yang, S. X., Zhang, H. Q., Liang, J. Q., Wang, H. B., and Lu, J. A. (2010). Gas Hydrate System of Shenhu Area, Northern South China Sea: Wire-Line Logging, Geochemical Results and Preliminary Resources Estimates. *2010 Offshore Technol. Conf.* 1 (1). (Houston, Texas, USA). doi:10.4043/20485-ms

Wu, N., Zhang, H., Yang, S., Zhang, G., Liang, J., Lu, J. a., et al. (2011). Gas Hydrate System of Shenhu Area, Northern South China Sea: Geochemical Results. *J. Geol. Res.* 2011, 1–10. doi:10.1155/2011/370298

Wu, P., Li, Y., Sun, X., Liu, W., and Song, Y. (2020). Mechanical Characteristics of Hydrate-Bearing Sediment: A Review. *Energy Fuels* 35 (2), 1041–1057. doi:10.1021/acs.energyfuels.0c03995

Yang, T., Jiang, S., Ge, L., Yang, J., Wu, N., Zhang, G., et al. (2010). Geochemical Characteristics of Pore Water in Shallow Sediments from Shenhu Area of South China Sea and Their Significance for Gas Hydrate Occurrence. *Chin. Sci. Bull.* 55 (8), 752–760. doi:10.1007/s11434-009-0312-2

Yang, L., Chen, C., Jia, R., Sun, Y., Guo, W., Pan, D., et al. (2018). Influence of Reservoir Stimulation on Marine Gas Hydrate Conversion Efficiency in Different Accumulation Conditions. *Energies* 11 (2), 339. doi:10.3390/en11020339

Yang, M., Gao, Y., Zhou, H., Chen, B., and Li, Y. (2019). Gas Production from Different Classes of Methane Hydrate Deposits by the Depressurization Method. *Int. J. Energ. Res.* 43 (10), 5493–5505. doi:10.1002/er.4669

Ye, J. L., Qin, X. W., Xie, W. W., Lu, H. L., Ma, B. J., Qiu, H. J., et al. (2020). The Second Natural Gas Hydrate Production Test in the South China Sea. *China Geol.* 2, 197–209. doi:10.31035/cg2020043

Yin, Z., Wan, Q.-C., Gao, Q., and Linga, P. (2020). Effect of Pressure Drawdown Rate on the Fluid Production Behaviour from Methane Hydrate-Bearing Sediments. *Appl. Energ.* 271, 115195. doi:10.1016/j.apenergy.2020.115195

Zhang, L., Yang, L., Wang, J., Zhao, J., Dong, H., Yang, M., et al. (2017). Enhanced CH4 Recovery and CO2 Storage via thermal Stimulation in the CH4/CO2 Replacement of Methane Hydrate. *Chem. Eng. J.* 308, 40–49. doi:10.1016/j.cej.2016.09.047

Zhao, J., Liu, D., Yang, M., and Song, Y. (2014). Analysis of Heat Transfer Effects on Gas Production from Methane Hydrate by Depressurization. *Int. J. Heat Mass Transfer* 77, 529–541. doi:10.1016/j.ijheatmasstransfer.2014.05.034

Zhao, E., Hou, J., Du, Q., Liu, Y., Ji, Y., and Bai, Y. (2021). Numerical Modeling of Gas Production from Methane Hydrate Deposits Using Low-Frequency Electrical Heating Assisted Depressurization Method. *Fuel* 290, 120075. doi:10.1016/j.fuel.2020.120075

Conflict of Interest: The authors declare that the research was conducted in the absence of any commercial or financial relationships that could be construed as a potential conflict of interest.

Publisher's Note: All claims expressed in this article are solely those of the authors and do not necessarily represent those of their affiliated organizations, or those of the publisher, the editors, and the reviewers. Any product that may be evaluated in this article, or claim that may be made by its manufacturer, is not guaranteed or endorsed by the publisher.